Supporting Material for:
SSMART: Sequence-structure motif identification for RNA-binding proteins

Alina Munteanu, Neelanjan Mukherjee, and Uwe Ohler

S1 Materials and Methods

S1.1 RNA secondary structure prediction

We considered two folding algorithms: RNAplfold (Bernhart *et al.*, 2006) and RNAprofiling (Rogers and Heitsch, 2014), and we compared their results on binding sites for two proteins with different structural preferences: PUM2, an RBP that prefers ss-RNA; and Staufen1, known to bind ds-RNA. We predicted RNA secondary structures for PUM2 and Staufen1 binding sites derived from *in vivo* PAR-CLIP and RIPiT data, respectively (Hafner *et al.*, 2010; Ricci *et al.*, 2014). We extended the core regions with maximum 25, 50, 75 or 150 nucleotides on each side, using either genomic coordinates in the case of intronic sequences, or the highest expressed isoform that contains the peak for the exonic ones. First, we compared RNAplfold predictions in multiple parameter settings, and then we compared the RNA secondary structure predictions of RNAplfold vs. RNAprofiling.

S1.1.1 RNAplfold predictions depend on parameters

RNAplfold is a tool from ViennaRNA package that predicts RNA single-strandedness using free energy minimization and locally stable secondary structures. It associates the best structure to each sliding window over the stretch of RNA of interest, and then outputs the average base pair probabilities. RNAplfold has two important parameters: the size of the window (W) and the maximum base pair span (L). Multiple applications of RNAplfold use the values $(W, L) = (80, 40)$ (see (Li *et al.*, 2010; Kazan *et al.*, 2010; Marin and Vanicek, 2011; Lekprasert *et al.*, 2011)), while (Lange *et al.*, 2012) recommend that $W = L + 50$ in order to have each base present in at least 51 windows.

We selected a wide range of parameters: $L \in [30, 150]$ and $W \in [L, L + 100]$, resulting in 143 (W, L) pairs, and we applied RNAplfold on 3974 PUM2 and 4666 Staufen1 peaks. In the folding step, we extended the peaks with maximum 150 bp on each side, after which we discarded the flanking regions and we analyzed only the initial binding sites with the associated RNA structures. Fig. S1 shows the percent of bases that were predicted to correspond to ds-RNA (bases that have the predicted unpaired probability < 0.5). RNAplfold predicts on average 13% more paired bases for Staufen1 binding sites than for PUM2 binding sites, a result consistent with the reported binding preferences for the two RBPs. We note that in both sets the results show a clear trend of more base pairs as the parameter values increase. This is also in agreement with the reported behaviour of multiple structure prediction tools, namely that the prediction accuracy for individual base-pairs decreases with respect to span length and/or window length (Doshi *et al.*, 2004; Kiryu *et al.*, 2011;

Lange *et al.*, 2012). Given this correlation between the parameter size and the percent of paired bases for both sets, it is unclear what the "optimal" parameter values might be. Looking at just two widely used parameter values, $(W, L) \in \{(80, 40), (150, 100)\}$, we observe an unsettling difference of 11.1% for PUM2 and 9.3% for Staufen1 in the number of paired RNA bases.

S1.1.2 Comparative analysis

Given the performance of RNAplfold with different parameter settings, we looked for another tool for RNA structure prediction, and we selected RNAprofiling, which has a different approach to RNA folding. RNAprofiling is an ensemble-based method that balance abstraction and specificity by identifying local dominant combinations of base pairs. It uses a statistical sample of 1000 RNA secondary structures from the Boltzmann ensemble of possible RNA secondary structures associated with a given RNA sequence. The tool then focuses on the arrangement of helices at the substructure level and reports the most frequent double-stranded regions. We consider a base to be paired only if it is contained in a helix that is present in more than half of the ensemble of secondary structures. RNAprofiling has no parameters, the results being influenced only by the length of the input sequence. We tested it with three different sizes for the flanking regions of the RBP binding sites: 25, 50 and 75 and we compared the results with RNAplfold predictions for $(W, L) \in \{(80, 40), (150, 100), (200, 150)\}$.

We used the Paired/Unpaired predictions to define the following similarity metric between two foldings a, b of the same sequence of length w:

$$Sim(a, b) = \frac{1}{w}\sum_{i=1}^{w} s_i, \text{ with } s_i = \begin{cases} 1, \text{ if } a_i \neq b_i \\ 0, \text{ if } a_i = b_i \end{cases} \tag{1}$$

where $a = \{a_1, a_2, \ldots, a_w\}$ and $b = \{b_1, b_2, \ldots, b_w\}$. A similarity score of 0 denotes identical structures, while a score of 0.3 means that the two predicted structures disagree in 30% of their positions. We compared the structures predicted by the two tools, each in three settings, for PUM2 and Staufen1 binding sites. The average similarity scores are depicted in Fig S2A. We note that the similarity between structure predictions for PUM2 (above the main diagonal) and Staufen1 (below the diagonal) has the same trend, with smaller values for comparisons between the same tool or between parameter settings with simmilar window lengths. The results that disagree the most (around 30%) correspond to the following pairs:

- RNAprofiling with shortest sequences (25 bp padding) & RNAplfold with the longest parameters ($W = 200, L = 150$), and
- RNAprofiling with longest sequences (75 bp padding) & RNAplfold with the shortest parameters ($W = 80, L = 40$).

The structural predictions that agree the most acros different tools (23-24%) correspond to simmilar folding sequences:

- short sequences: RNAprofiling with 25 bp padding & RNAplfold with $W = 80, L = 40$, and
- mid-range sequence: RNAprofiling with 50 bp padding & RNAplfold with $W = 150, L = 100$.

We also analyzed the percent of bases that were predicted to correspond to ds-RNA (Fig S2B). Staufen1 binding sites have an average 12% more paired bases than PUM2 sites, a trend consistent with the binding preferences shown by these RBPs. However, the secondary structure predicted by RNAplfold is correlated with the parameters used, longer values yielding more paired bases, while RNAprofiling predictions are quite stable with respect to the length of flanks.

We used RNAprofiling for all **SSMART** results reported here, but the user can compute secondary structures with any tool, if then the predicted structures are properly encoded into the input sequences. In order to predict secondary structures relevant to the experimental data, we apply the folding algorithm either on the RNA oligos in the case of RNAcompete data, or on extended peaks in the case of CLIP datasets (±50 bp). The extension is performed using either genomic coordinates in the case of intronic sequences, or the highest expressed isoform (from RNA-seq data) that contains the peak for the exonic ones. The extended RNA sequences are used only in the structure prediction step, after which only the core sequences are associated with the secondary structures in **SSMART** input files.

S1.2 The objective function in regression setting

The random set scoring function used by **SSMART** is defined by:

$$S^{RS}(m_j) = \frac{\frac{1}{n_j}\sum_{i:x_{ij}=1} y_i - \mu}{\sigma_j} \tag{2}$$

$$\mu = \frac{1}{n}\sum_{i=1}^{n} y_i, \sigma_j^2 = \frac{n-n_j}{n_j(n-1)}\left[\frac{1}{n}\sum_i y_i^2 - \left(\frac{1}{n}\sum_i y_i\right)^2\right]$$

The associated optimization problem is:

$$\hat{m}^{RS} = \underset{m_j \in M}{\arg\max}\, S^{RS}(m_j) \tag{3}$$

where M is the set of putative motifs $\{m_1, \ldots, m_p\}$, and $\hat{m}^{RS}$ is the best guess at the optimal binding motif m^*.

Another approach is to use a regression score (LR score). This is more computationally demanding but can account for some, potentially relevant, confounder information, like di-nucleotide frequencies or sequence length. In order to describe the regression framework, we will rewrite the random set score from Eq. (2). We make the following notations:

$$\mu = \frac{1}{n}\sum_{i=1}^{n} y_i, \qquad \sigma^2 = \frac{1}{n}\sum_{i=1}^{n}(y_i-\mu)^2$$

$$y_i^* = y_i - \mu, \qquad A_j = \frac{n-n_j}{n-1}$$

$$e_j = \frac{1}{n_j}\sum_{i:x_{ij}=1} y_i^*, \qquad \hat{\sigma_j}^2 = \frac{\sigma^2}{n_j}$$

Then we have

$$S^{RS}(m_j) = A_j \times \frac{e_j}{\hat{\sigma_j}} \tag{4}$$

with the top predicted motif $\hat{m}^{RS}$ described by Eq. (3).

Now we can define a linear regression model for the binding interactions, that closely resembles the random set scoring strategy described above. Let the regression coefficient for motif m_j be denoted β_j, then a simple linear model for binding is:

$$y_i^* = x_{ij}\beta_j + \epsilon_i, \text{with } \epsilon_i \sim N(0, \sigma^2) \tag{5}$$

We estimate the regression coefficient with classical ordinary least squares (OLS): $\beta_j^{OLS} = \frac{1}{n_j}\sum_{i:x_{ij}=1} y_i^*$ and we define the motif enrichment score as follows:

$$S^{LR}(m_j) = \frac{\beta_j^{OLS}}{\hat{\sigma_j}} = \frac{1}{A_j} \times S^{RS}(m_j) \tag{6}$$

The top motif is in this case:

$$\hat{m}^{LR} = \arg\max_{m_j \in M} S_j^{LR} \tag{7}$$

Note that if the size of the motif target set is small relative to the number of all input sequences ($n_j << n$), $A_j \approx 1$ and $S_j^{LR} \approx S_j^{RS}$.

This framework can be extended to account for features of the input sequences that may be unrelated to motif binding. One such potential confounder is the sequence length, and other important features can be derived from the nucleotide content, like the di-nucleotide counts. If we consider q additional confounders, the regression covariates for motif m_j are defined by the following matrix: $Z_j = (x_j, c_1, c_2, \ldots, c_q)$, where x_j represents the column vector of motif matches x_{ij}, and $c_k \in \mathbb{R}^n, k \in \{1, \ldots, q\}$ are the confounders. We denote the corresponding regression coefficients with $\beta_{0j}, \beta_{1j}, \ldots \beta_{qj}$, with $\beta_{kj} \in \mathbb{R}, k \in \{0, \ldots, q\}$. Then the model can be expressed with the matrix notation as:

$$Y^* = Z_j\beta_j + \epsilon, \text{where } \epsilon \sim N(0, \sigma^2 I_{n\times n}) \tag{8}$$

In the typical case there are a large number of input sequences and therefore a large number of sample points to use in the estimation process. Also, we need to score a large number of motif candidates, therefore we need a computationally efficient estimator for the regression coefficients, with good statistical properties. We use the simple OLS estimator $\beta_j^{OLS} = (Z_j^T Z_j)^{-1} Z_j^T Y^*$, that provide fast solutions for small to moderate q values. The corresponding motif scoring function is a straightforward generalization of the univariate regression case:

$$S^{LR}(m_j) = \frac{\beta_j^{OLS}}{\hat{\sigma_j}}, \text{with } \hat{\sigma_j}^2 = (\hat{\Sigma}_{\hat{\beta_j}})_{11} \tag{9}$$

where $(\hat{\Sigma}_{\hat{\beta_j}})_{11}$ represents the first diagonal element in the covariance matrix for the parameter estimate β_j^{OLS}.

We optimized this scoring function in the case of the analyzed CLIP datasets, using as confounders the sequence length and the di-nucleotide counts. For the RNAcompete datasets we optimized the random set scoring function since all the input RNA sequences have the same length and were generated artificially with an uniform model.

S1.3 Update rules in the search strategy

Given a motif m, a set of candidate motifs is constructed by applying small variations to m: in length, sequence, or structure. The k-mer m is extended to 16 new $(k+1)$-mers, by independently adding one letter from A_{basic} at one of its end. If $k > 4$, the length of the motif is reduced and 2 new $(k-1)$-mers are considered. Then a large set of new k-mers are obtained by changing one letter at a time in terms of structural change or increasing/decreasing sequence degeneracy. Briefly, for each position j in m, the following rules are applied:

- if $m[j] \in \{A, C, G, T, a, c, g, t\}$ then four new motif candidates are constructed by replacing $m[j]$, in turns, with its structural complement and the three letters that encode for it and one other nucleotide, keeping the original structure; for example A will become a, M, R, W, and g will become G, k, r, s;
- if $m[j] \in \{W, K, R, Y, S, M, w, k, r, y, s, m\}$ then three new k-mers are obtained with $m[j]$ set to either its structural complement, or to one of the nucleotides it encodes, in the same structural context; for example R will become r, A, G;
- if $m[j] \in \{W, K, R, Y, S, M, w, k, r, y, s, m\}$ and $j \notin \{1, k\}$ then a fourth candidate is obtained by setting $m[j] = N$ or $m[j] = n$, depending on the case;
- if $m[j] \in \{N, n\}$ then 10 new motifs are considered by changing $m[j]$ to one letter from either $\{A, C, G, T, W, K, R, Y, S, M\}$, or $\{a, c, g, t, w, k, r, y, s, m\}$.

For example $(4k + 18)$ candidate motifs are generated for a k-mer with no sequence degeneracies, or for a k-mer with double degeneracy in two middle positions. In the case of a k-mer with double degeneracy at its ends, $(4k + 16)$ new motifs are considered.

S1.4 Visualization of motif clusters

The k-mer motifs obtained in the search procedure are then clustered in a post-processing step. For a better understanding of this step, **SSMART** plots all unique evolved motifs and the similarity between them in two ways: as a heatmap and as a network graph (see Fig. S3). The similarity is computed with the metric defined for the post-processing step. The heatmap plot depicts all pair-wise similarities between the evolved k-mers, together with their hierarchical clustering. The network graph provides a different perspective of the same data, filtering out the low similarities. In both the heatmap and the network graph the motifs are colored according to the motif cluster they belong to after the custom clustering procedure.

Fig. S3 contains the visualization of k-mers similarity for two libraies corresponding to PUM2 and FUS proteins. While for PUM2 the evolved motifs are more homogeneous, the ones for FUS apear to be more disperse. Depending of the data, there can be small motif clusters (like Motif2 of PUM2 with 4 k-mers or Motif3 of FUS with 5 k-mers), or clusters that incorporate many evolved motifs (like the top PUM2 motif that contains almost half of the k-mers).

S1.5 Parameter optimization

While our tool and *Zagros* do not have parameters that need to be set, *RNAcontext* and *GraphProt* have multiple parameters that influence their performance.

RNAcontext has three important parameters: the motif length w, the structural alphabet e and the number of initializations s. The motif length is specified as a range, and *RNAcontext* uses learned models for smaller motifs to initialize longer motif lengths. We set w to $4 - 10$, a range that is consistent with the **SSMART** possible motif lengths. For describing RNA structure, we used the "PHIME" alphabet that consists of five different structures: paired (P), hairpin loop (H), internal loop (I), multiloop (M), and external loop (E). For structure evaluations we considered the paired probabilities. We set parameter s to 3, running the tool with 3 different initializations.

GraphProt has six parameters that can be optimized in a dedicated step, using program option $-ls$. For each motif and type of structure used in the synthetic datasets, we ran the optimization procedure on a separate set of sequences and used the optimized values for all datasets in each category. However, the motif recovery rates with the default parameters were better than those obtained with prior parameter optimization (see Table S3), therefore all results reported in the main text correspond to the default values.

S1.6 Amount of noise in the synthetic data

In our analyses we generated synthetic datasets that contain specific implanted motifs in various proportions of structured/unstructured binding sites. In addition to the "positive" sequences, we added some noise to each of our 2000 datasets. While for the "primary" synthetic datasets we added in each case 500 noise sequences, as described in the main text, we also generated "secondary" sets with the same positives, but with only 200 noise sequences. When we randomly associated binding scores to sequences in the second datasets, we chose a different distribution, making sure that the 200 noise sequences will be in the bottom 400 scores. Throughtout the paper, the implicit synthetic datasets are the "primary" sets.

The comparison of tool performance on the synthetic datasets with different amount and distribution of noise is presented in Table **??**. For all tools, the recovery rates are better for the case with less noise, but the difference is ussualy bellow 3%. The only exception is *RNAcontext*, with a 15% drop in sequence motif recovery for the "primary" datasets (2000 positives & 500 negatives).

S2 Supplementary figures and tables

Table S1: 10 randomly selected PWMs from the RBP compendium. These PWM were used to generate the synthetic datasets used for evaluation. IC refers to information content.

Motif	Average IC	Consensus	RBP
M159_0.6	1.4693	WGCAUGM	A2BP1, RBFOX2, RBFOX3
M147_0.6	1.3348	GACAGAN	CNOT4
M056_0.6	1.253	ACAACRR	SRSF3
M021_0.6	1.2086	AGGAURA	G3BP2
M232_0.6	1.1782	UUUUUUU	ELAVL1, ELAVL3
M162_0.6	1.0972	AGAAANU	PABPC5
M108_0.6	1.0967	UUUGUUU	ELAVL1, ELAVL3
M242_0.6	1.0365	CCAAAUU	HNRNPR, SYNCRIP
M054_0.6	0.9501	GCGCGCG	RBM8A
M168_0.6	0.6589	GURGUKU	PSPC1, SFPQ

Table S2: Biological datasets used in the main text of the manuscript to compare motifs recovered from *in vivo* and *in vitro* data.

Protein	CLIP SRA accession number	RNAcompete ID
ELAVL1	SRR189777	RNCMPT00032
QKI	SRR048969	RNCMPT00047
FMR1	SRR527727	RNCMPT00016
LIN28A	SRR531465	RNCMPT00162
LIN28A	SRR458759	
LIN28A	SRR764666	
FUS	SRR070449	RNCMPT00018
PUM2	SRR048968	
ROQUIN	SRR857933	

Table S3: Comparison of motif recovery rates for *GraphProt* and *Zagros* obtained with default parameters and/or in sequence-only mode. All results correspond to the secondary set of synthetic data, each dataset with 2000 positives and 200 negatives.

Motif	*GraphProt*			*Zagros*	
	With param. optimization	Default params	Default params & sequence-only	Sequence-structure mode	Sequence-only
Sequence	93.65	97.4	95.2	100	96.1
Structure	72.3	74.45	20.55	19.35	24.3

Table S4: Comparison of motif recovery rates on two set of synthetic data: the primary one having datasets with 2000 positives and 500 negatives (in a triangular distribution), and the secondary one having datasets with 2000 positives and 200 negatives (situated among the bottom 400 sequences).

Motif	Synthetic data	SSMART	SSMART-seq	RNAcontext	GraphProt	Zagros
Sequence	2000 pos & 500 neg (triang)	91.75	92.05	58.14	94.84	100
Sequence	2000 pos & 200 neg (bottom)	92.2	94.59	73.2	97.4	100
Structure	2000 pos & 500 neg (triang)	88.65	14.75	50.03	73.25	15.25
Structure	2000 pos & 200 neg (bottom)	89.2	22.23	56.3	74.45	19.35

Table S5: The cutoffs used to distinguish between "recovered" and "not recovered" motifs on two set of synthetic data: (A) for the primary synthetic data (2000 positives and 500 negatives), and (B) the secondary synthetic data (2000 positives and 200 negatives). The tools marked with "-seq" correspond to sequence-only mode, while the "*" marks the *GraphProt* run with optimized parameters.

A)

Motif finder	Sequence	Structure
SSMART	0.8082	0.7188
SSMART-seq	0.8206	0.8725
RNAcontext	0.6995	0.7366
GraphProt	0.6599	0.8232
Zagros	0.817	0.8908

B)

Motif finder	Sequence	Structure
SSMART	0.8115	0.7095
SSMART-seq	0.8095	0.7607
RNAcontext	0.7008	0.7359
GraphProt	0.6602	0.8175
GraphProt*	0.6514	0.8222
GraphProt-seq	0.5874	0.7551
Zagros	0.818	0.8659
Zagros-seq	0.9092	0.7448

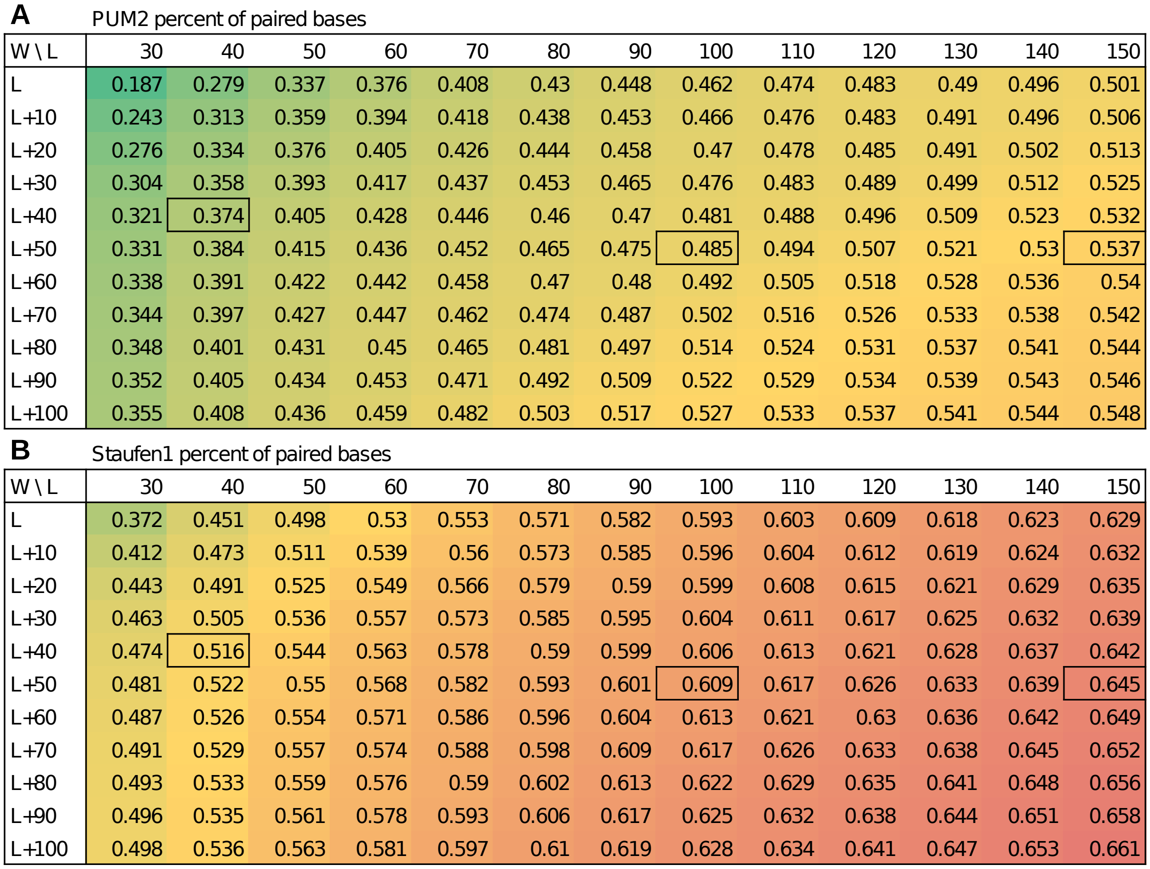

A PUM2 percent of paired bases

W \ L	30	40	50	60	70	80	90	100	110	120	130	140	150
L	0.187	0.279	0.337	0.376	0.408	0.43	0.448	0.462	0.474	0.483	0.49	0.496	0.501
L+10	0.243	0.313	0.359	0.394	0.418	0.438	0.453	0.466	0.476	0.483	0.491	0.496	0.506
L+20	0.276	0.334	0.376	0.405	0.426	0.444	0.458	0.47	0.478	0.485	0.491	0.502	0.513
L+30	0.304	0.358	0.393	0.417	0.437	0.453	0.465	0.476	0.483	0.489	0.499	0.512	0.525
L+40	0.321	0.374	0.405	0.428	0.446	0.46	0.47	0.481	0.488	0.496	0.509	0.523	0.532
L+50	0.331	0.384	0.415	0.436	0.452	0.465	0.475	0.485	0.494	0.507	0.521	0.53	0.537
L+60	0.338	0.391	0.422	0.442	0.458	0.47	0.48	0.492	0.505	0.518	0.528	0.536	0.54
L+70	0.344	0.397	0.427	0.447	0.462	0.474	0.487	0.502	0.516	0.526	0.533	0.538	0.542
L+80	0.348	0.401	0.431	0.45	0.465	0.481	0.497	0.514	0.524	0.531	0.537	0.541	0.544
L+90	0.352	0.405	0.434	0.453	0.471	0.492	0.509	0.522	0.529	0.534	0.539	0.543	0.546
L+100	0.355	0.408	0.436	0.459	0.482	0.503	0.517	0.527	0.533	0.537	0.541	0.544	0.548

B Staufen1 percent of paired bases

W \ L	30	40	50	60	70	80	90	100	110	120	130	140	150
L	0.372	0.451	0.498	0.53	0.553	0.571	0.582	0.593	0.603	0.609	0.618	0.623	0.629
L+10	0.412	0.473	0.511	0.539	0.56	0.573	0.585	0.596	0.604	0.612	0.619	0.624	0.632
L+20	0.443	0.491	0.525	0.549	0.566	0.579	0.59	0.599	0.608	0.615	0.621	0.629	0.635
L+30	0.463	0.505	0.536	0.557	0.573	0.585	0.595	0.604	0.611	0.617	0.625	0.632	0.639
L+40	0.474	0.516	0.544	0.563	0.578	0.59	0.599	0.606	0.613	0.621	0.628	0.637	0.642
L+50	0.481	0.522	0.55	0.568	0.582	0.593	0.601	0.609	0.617	0.626	0.633	0.639	0.645
L+60	0.487	0.526	0.554	0.571	0.586	0.596	0.604	0.613	0.621	0.63	0.636	0.642	0.649
L+70	0.491	0.529	0.557	0.574	0.588	0.598	0.609	0.617	0.626	0.633	0.638	0.645	0.652
L+80	0.493	0.533	0.559	0.576	0.59	0.602	0.613	0.622	0.629	0.635	0.641	0.648	0.656
L+90	0.496	0.535	0.561	0.578	0.593	0.606	0.617	0.625	0.632	0.638	0.644	0.651	0.658
L+100	0.498	0.536	0.563	0.581	0.597	0.61	0.619	0.628	0.634	0.641	0.647	0.653	0.661

Figure S1: RNAplfold predictions with different values for parameters W (window length) and L (maximum base pair span). The numbers presented in a heatmap-like manner correspond to the percent of paired nucleotides. The values in boxes correspond to three parameter settings widely used in the literature: $(W, L) \in \{(80, 40), (150, 100), (200, 150)\}$. (A) Predictions for PUM2 binding sites. (B) Predictions for Staufen1 binding sites.

Table S6: CLIP datasets used in the main text of the manuscript to compare different motif finders.

Protein	Protocol	Cell line	Reference	SRR accession number	ID
ELAVL1	PAR-CLIP	HEK293	Kishore *et al.* (2011)	SRR189777	ELAVL1.1
ELAVL1	PAR-CLIP	HEK293	Mukherjee *et al.* (2011)	SRR248532	ELAVL1.2
ELAVL1	PAR-CLIP	HeLa	Lebedeva *et al.* (2011)	SRR309285	ELAVL1.3A
ELAVL1	PAR-CLIP	HeLa	Lebedeva *et al.* (2011)	SRR309286	ELAVL1.3B
PUM2	PAR-CLIP	HEK293	Hafner *et al.* (2010)	SRR048967	PUM2.A
PUM2	PAR-CLIP	HEK293	Hafner *et al.* (2010)	SRR048968	PUM2.B

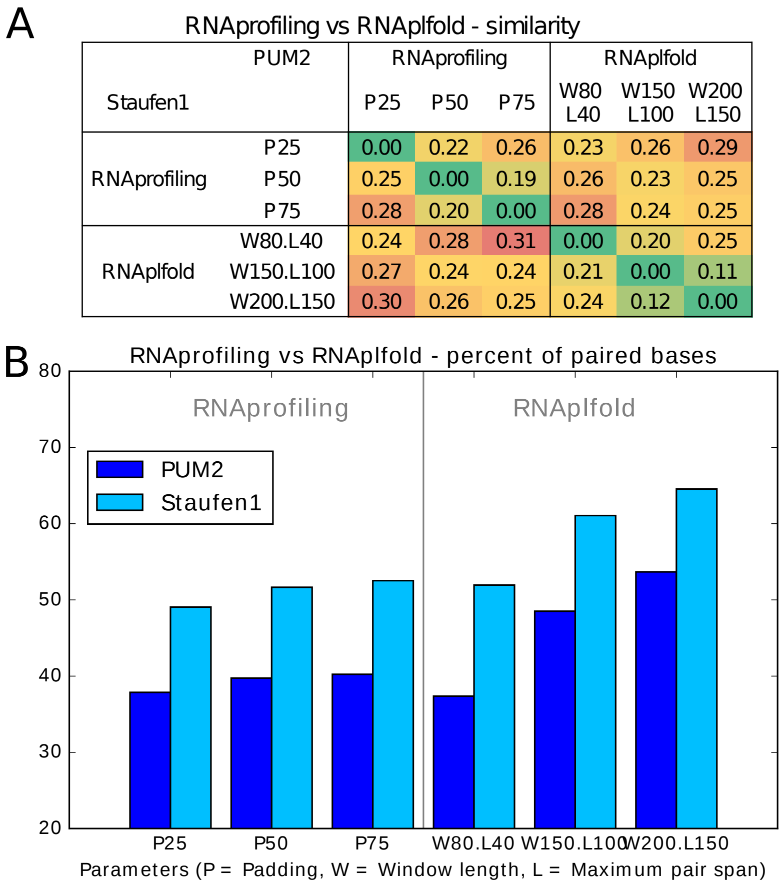

Staufen1	PUM2	RNAprofiling			RNAplfold		
		P25	P50	P75	W80 L40	W150 L100	W200 L150
RNAprofiling	P25	0.00	0.22	0.26	0.23	0.26	0.29
	P50	0.25	0.00	0.19	0.26	0.23	0.25
	P75	0.28	0.20	0.00	0.28	0.24	0.25
RNAplfold	W80.L40	0.24	0.28	0.31	0.00	0.20	0.25
	W150.L100	0.27	0.24	0.24	0.21	0.00	0.11
	W200.L150	0.30	0.26	0.25	0.24	0.12	0.00

Figure S2: RNAprofiling vs RNAplfold in different parameter settings (P = Padding, W = Window length, L = Maximum pair span). (A) Average similarity between predicted structures. The values above the diagonal correspond to PUM2, while the values below the diagonal correspond to Staufen1. (B) Percent of paired bases for PUM2 and Staufen1 binding sites.

Table S7: P-values obtained with two-sample Kolmogorov-Smirnov tests on the Kendall tau correlation coeficients for the motifs predicted for one specific RBP. The comparison is performed between correlation of the motifs with datasets for the same protein and with datasets for the other considered RBP.

Tool	ELAVL1 seq motifs	PUM2 seq motifs	ELAVL1 seq-struct motifs	PUM2 seq-struct motifs
SSMART	0.0001604	0.002797	0.0001604	0.002797
GraphProt	0.000002719	0.3357	0.00002447	0.002797
Zagros	0.000002719	0.06154	0.1256	0.002797

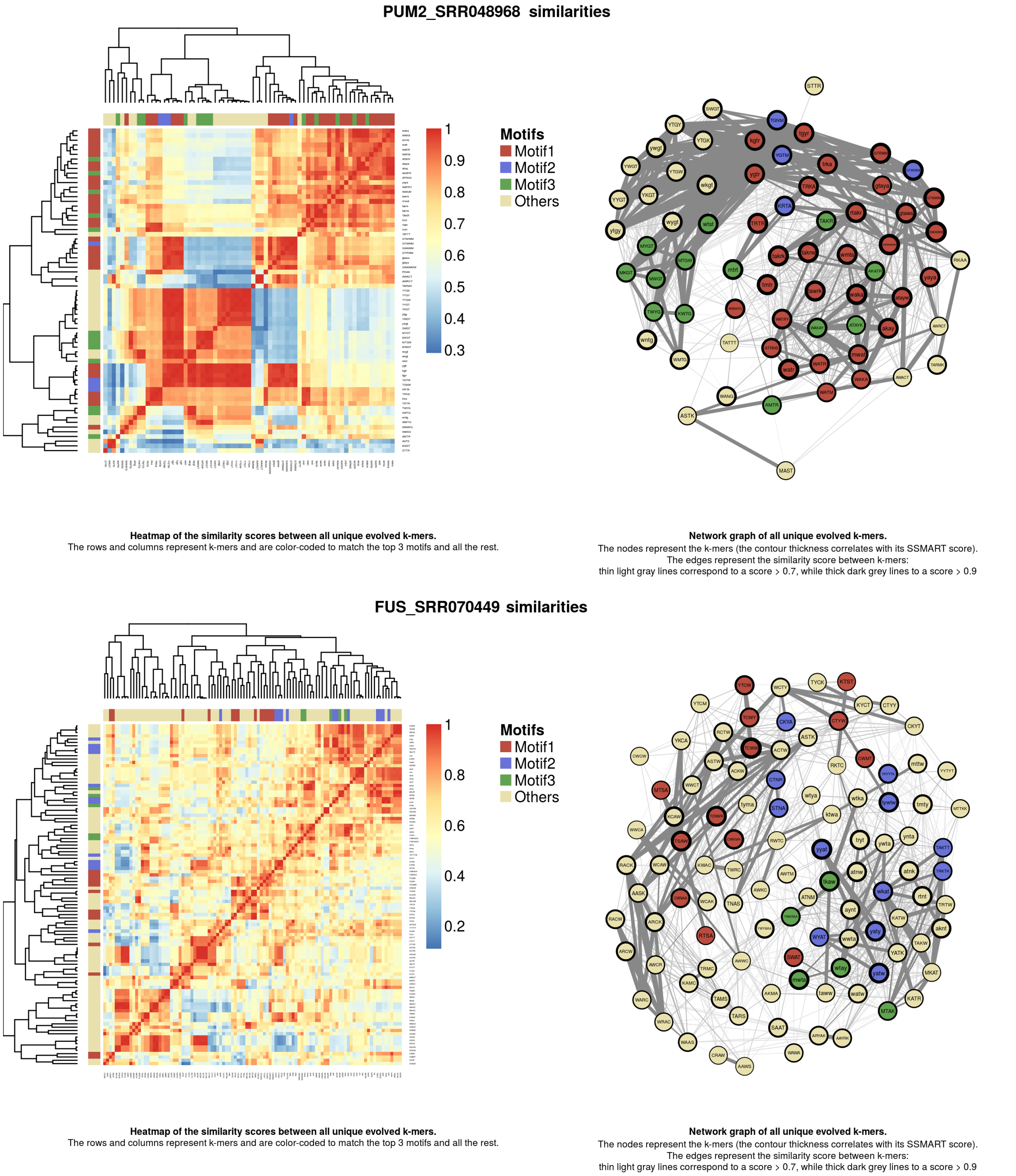

Heatmap of the similarity scores between all unique evolved k-mers.
The rows and columns represent k-mers and are color-coded to match the top 3 motifs and all the rest.

Network graph of all unique evolved k-mers.
The nodes represent the k-mers (the contour thickness correlates with its SSMART score).
The edges represent the similarity score between k-mers:
thin light gray lines correspond to a score > 0.7, while thick dark grey lines to a score > 0.9

Heatmap of the similarity scores between all unique evolved k-mers.
The rows and columns represent k-mers and are color-coded to match the top 3 motifs and all the rest.

Network graph of all unique evolved k-mers.
The nodes represent the k-mers (the contour thickness correlates with its SSMART score).
The edges represent the similarity score between k-mers:
thin light gray lines correspond to a score > 0.7, while thick dark grey lines to a score > 0.9

Figure S3: Visualization of motif clusters. Data corresponds to PUM2 (top) and FUS (bottom) proteins. The panel for each RBP contains a heatmap (left) and a network graph (right). Both plots depict the pair-wise similarities between all unique evolved motifs (k-mers). The k-mers are represented on rows and columns in the heatmap plot and as nodes in the network graph. They are color-coded to match the motif cluster they are assign to in the post-processing step. In the network graph, two motifs are connected by an edge if they have more than 90% similarity (thick dark grey edge) or between 70%-90% similarity (thin light grey line). Similarities bellow 70% are not depicted in this plot.

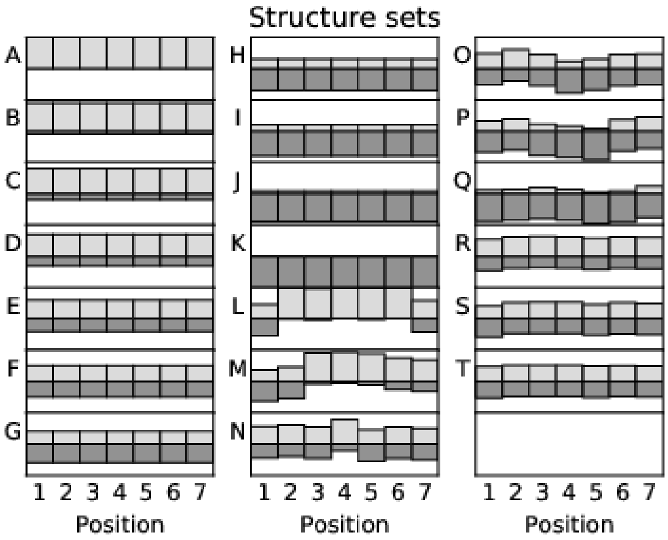

Figure S4: Structural environments in synthetic data. The overall structure that corresponds to the 10 datasets generated for motif M147 is depicted for each type of structure A-T. For each position in the motif, the light grey rectangle coresponds to the probability of being unpaired, while the dark grey represents the paired probability.

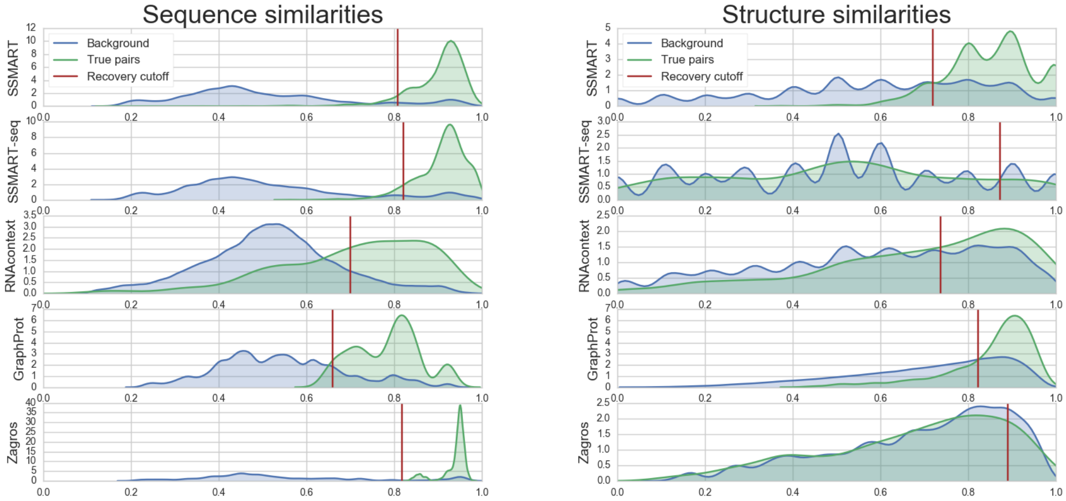

Figure S5: Distribution of similarity scores between predicted and implanted motifs in synthetic datasets. The scores correspond to sequence motifs (left) and structure motifs (right). The similarities computed for all synthetic sets are depicted in green (True pairs), while the background consisting in the similarities between at possible pairs of predicted and implanted motifs are represented in blue. The vertical brown line represents the optimized cuttof for each tool. All motifs that have scores to the rigth of this line are considered "recovered" by the motif finder.

S3 SSMART results on RNAcompete datasets

The results reported here were obtained using **SSMART** 1.2 with the random set scoring function, since it is fast and there is no need to acount for covariates. All oligos from an RNAcompete experiment have the same length and were designed with a uniform nucleotide distribution.

Table S8: Selected list of RNAcompete datasets on which **SSMART** was applied. They correspond to the selected RBPs for the comparison between motif predictions on *in vivo* and *in vitro* data.

Protein	RNAcompete ID	GEO ID	Results ID
FMR1	RNCMPT00016	GSM1011721	FMR1 RNCMPT00016
FUS	RNCMPT00018	GSM1011691	FUS RNCMPT00018
FXR1	RNCMPT00161	GSM1011671	FXR1 RNCMPT00161
FXR2	RNCMPT00020	GSM1011674	FXR2 RNCMPT00020
IGF2BP2	RNCMPT00033	GSM1011697	IGF2BP2 RNCMPT00033
IGF2BP3	RNCMPT00172	GSM1011694	IGF2BP3 RNCMPT00172
ELAVL1	RNCMPT00032	GSM1011629	ELAVL1 RNCMPT00032
ELAVL1	RNCMPT00112	GSM1011563	ELAVL1 RNCMPT00112
ELAVL1	RNCMPT00117	GSM1011582	ELAVL1 RNCMPT00117
ELAVL1	RNCMPT00136	GSM1011621	ELAVL1 RNCMPT00136
ELAVL1	RNCMPT00274	GSM1138954	ELAVL1 RNCMPT00274
LIN28A	RNCMPT00162	GSM1011679	LIN28A RNCMPT00162
QKI	RNCMPT00047	GSM1011730	QKI RNCMPT00047
SRSF1	RNCMPT00106	GSM1011565	SF2 RNCMPT00106
SRSF1	RNCMPT00107	GSM1011574	SF2 RNCMPT00107
SRSF1	RNCMPT00108	GSM1011594	SF2 RNCMPT00108
SRSF1	RNCMPT00109	GSM1011595	SF2 RNCMPT00109
SRSF1	RNCMPT00110	GSM1011637	SF2 RNCMPT00110
SRSF7	RNCMPT00073	GSM1011738	SRSF7 RNCMPT00073
SRSF9	RNCMPT00067	GSM1011666	SFRS9 RNCMPT00067
SRSF9	RNCMPT00074	GSM1011739	SRSF9 RNCMPT00074

Protein ID	Reported motif	**SSMART** top 3 sequence-structure motifs		
FMR1 RNCMPT00016	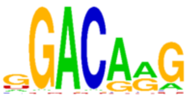	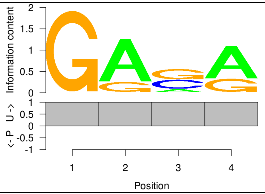	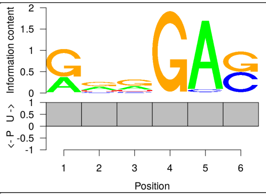	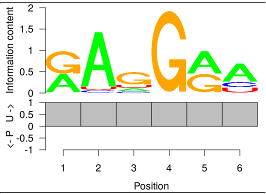
FUS RNCMPT00018	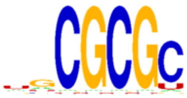	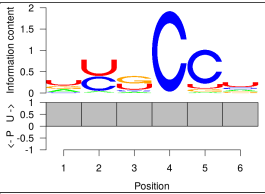	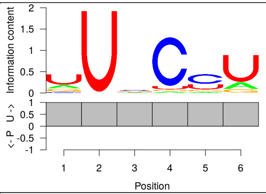	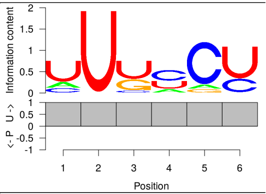
ELAVL1 RNCMPT00032	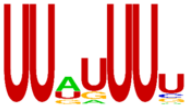	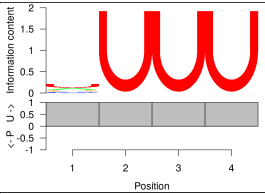	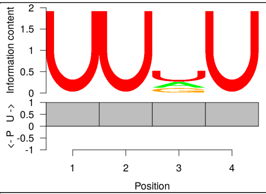	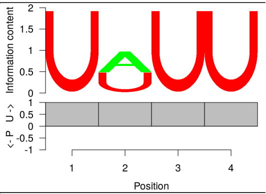
ELAVL1 RNCMPT00112	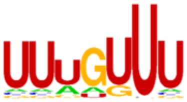	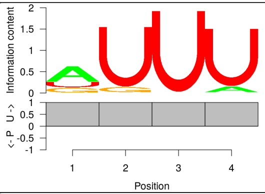	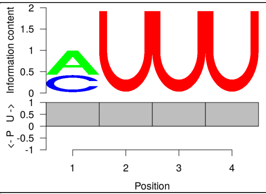	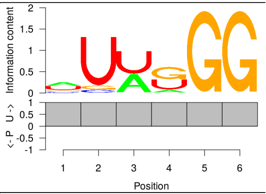
ELAVL1 RNCMPT00117	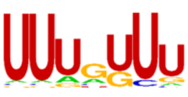	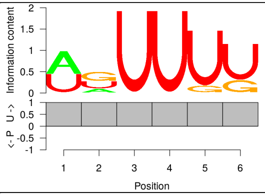	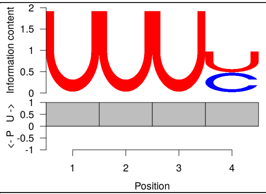	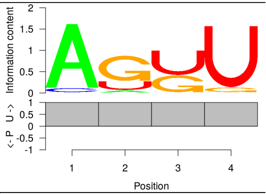
ELAVL1 RNCMPT00136	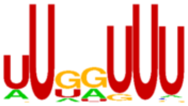	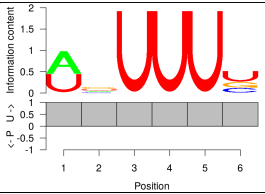	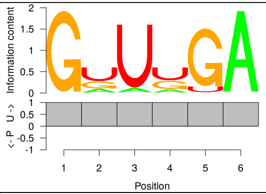	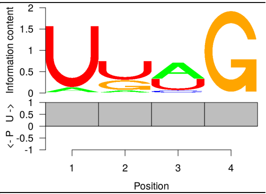
ELAVL1 RNCMPT00274	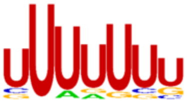	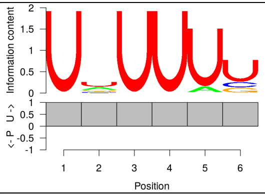	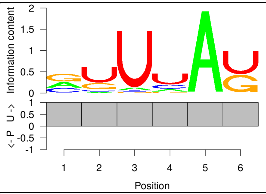	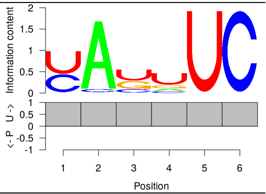
IGF2BP2 RNCMPT00033	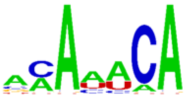	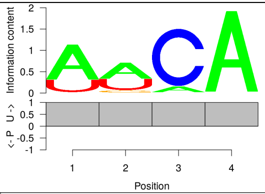	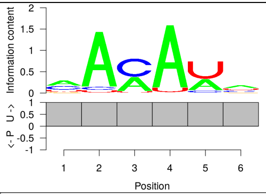	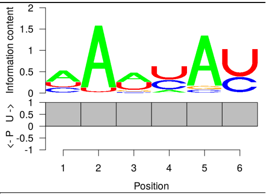
IGF2BP3 RNCMPT00172	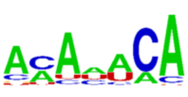	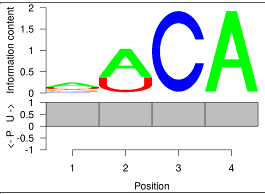	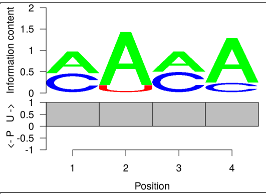	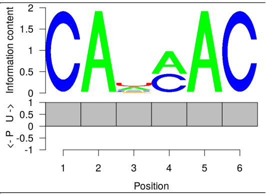
LIN28A RNCMPT00162	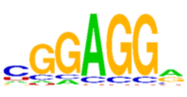	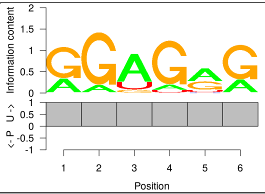	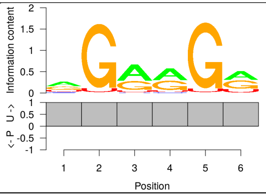	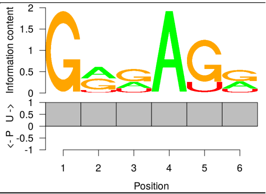

Protein ID	Reported motif	**SSMART** top 3 sequence-structure motifs
QKI RNCMPT00047	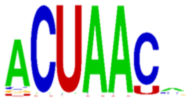	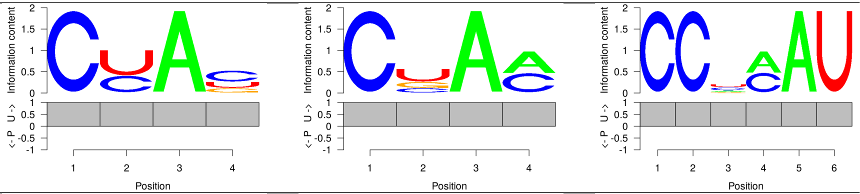
SF2 RNCMPT00106	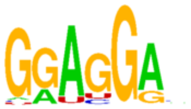	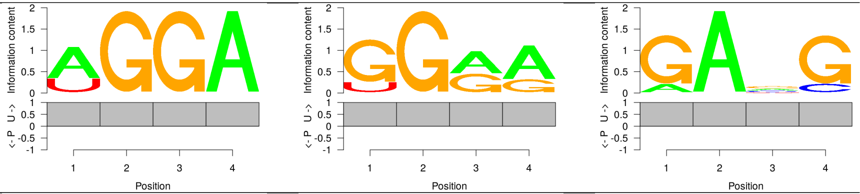
SF2 RNCMPT00107	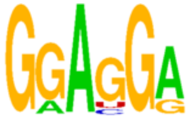	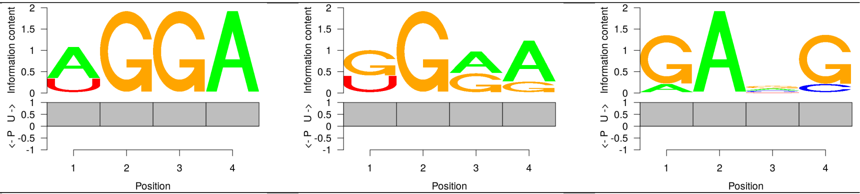
SF2 RNCMPT00108	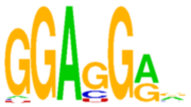	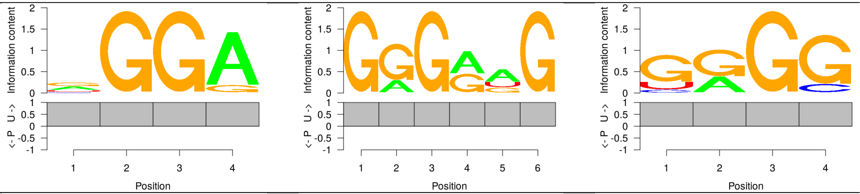
SF2 RNCMPT00109	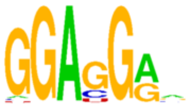	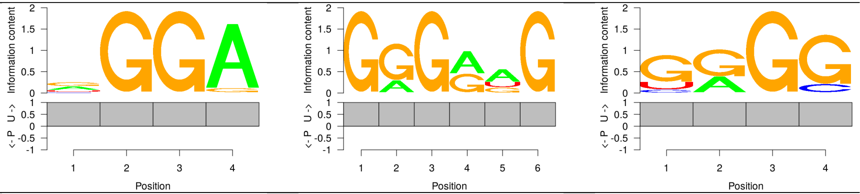
SF2 RNCMPT00110	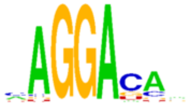	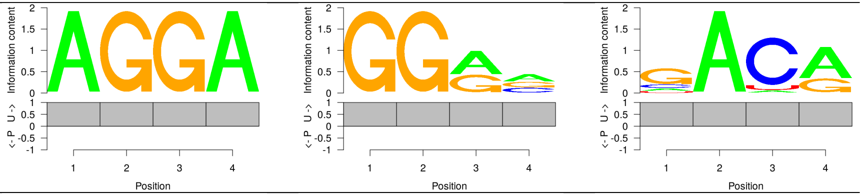
SRSF7 RNCMPT00073	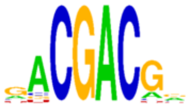	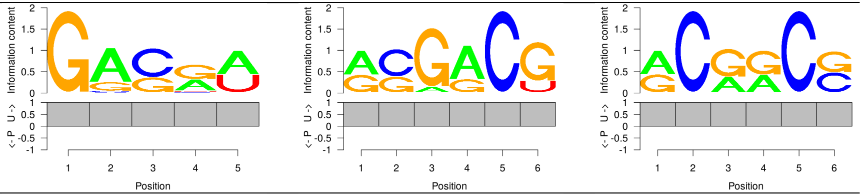
SFRS9 RNCMPT00067	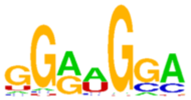	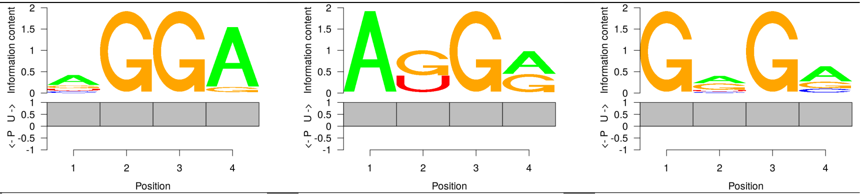
SRSF9 RNCMPT00074	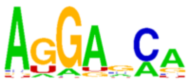	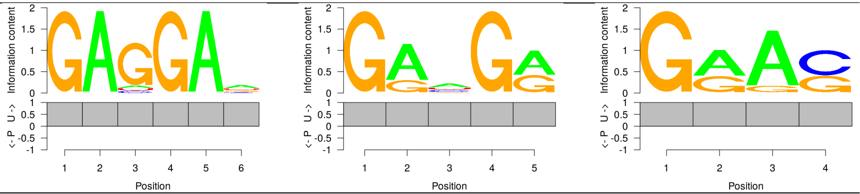

S4 SSMART results on CLIP datasets

The results reported here were obtained using **SSMART** 1.2 with the regression scoring.

Table S9: Full list of CLIP datasets on which **SSMART** was applied.

Protein	Paper	SRA accession number	Protocol	Cell line	Results ID
FMR1	Ascano *et al.* (2012)	SRR527727	PAR-CLIP	HEK293	FMR1 SRR527727
FMR1	Ascano *et al.* (2012)	SRR527728	PAR-CLIP	HEK293	FMR1 SRR527728
FUS	Hoell *et al.* (2011)	SRR070449	PAR-CLIP	HEK293	FUS SRR070449
FUS	Hoell *et al.* (2011)	SRR070450	PAR-CLIP	HEK293	FUS SRR070450
ELAVL1	Kishore *et al.* (2011)	SRR189777	PAR-CLIP	HEK293	ELAVL1 SRR189777
ELAVL1	Mukherjee *et al.* (2011)	SRR248532	PAR-CLIP	HEK293	ELAVL1 SRR248532
ELAVL1	Lebedeva *et al.* (2011)	SRR309285	PAR-CLIP	HeLa	ELAVL1 SRR309285
ELAVL1	Lebedeva *et al.* (2011)	SRR309286	PAR-CLIP	HeLa	ELAVL1 SRR309286
IGF2BP2	Hafner *et al.* (2010)	SRR048957	PAR-CLIP	HEK293	IGF2BP2 SRR048957
IGF2BP2	Hafner *et al.* (2010)	SRR048958	PAR-CLIP	HEK293	IGF2BP2 SRR048958
IGF2BP2	Hafner *et al.* (2010)	SRR048959	PAR-CLIP	HEK293	IGF2BP2 SRR048959
IGF2BP3	Hafner *et al.* (2010)	SRR048962	PAR-CLIP	HEK293	IGF2BP3 SRR048962
IGF2BP3	Hafner *et al.* (2010)	SRR048963	PAR-CLIP	HEK293	IGF2BP3 SRR048963
IGF2BP3	Hafner *et al.* (2010)	SRR048964	PAR-CLIP	HEK293	IGF2BP3 SRR048964
LIN28A	Cho *et al.* (2012)	SRR458758	CLIP-seq	A3-1	LIN28A-mm SRR458758
LIN28A	Cho *et al.* (2012)	SRR458759	CLIP-seq	A3-1	LIN28A-mm SRR458759
LIN28A	Cho *et al.* (2012)	SRR458760	CLIP-seq	A3-1	LIN28A-mm SRR458760
LIN28A	Wilbert *et al.* (2012)	SRS352780	CLIP-seq	H9	LIN28A SRS352780
LIN28A	Wilbert *et al.* (2012)	SRR531465	CLIP-seq	HEK293	LIN28A SRR531465
LIN28A	Hafner *et al.* (2013)	SRR764666	PAR-CLIP	HEK293	LIN28A SRR764666
LIN28B	Graf *et al.* (2013)	SRR850551	PAR-CLIP	HEK293	LIN28B SRR850551
LIN28B	Graf *et al.* (2013)	SRR850552	PAR-CLIP	HEK293	LIN28B SRR850552
LIN28B	Hafner *et al.* (2013)	SRR764667	PAR-CLIP	HEK293	LIN28B SRR764667
LIN28B	Hafner *et al.* (2013)	SRR764668	PAR-CLIP	HEK293	LIN28B SRR764668
LIN28B	Hafner *et al.* (2013)	SRR764669	PAR-CLIP	HEK293	LIN28B SRR764669
PUM2	Hafner *et al.* (2010)	SRR048967	PAR-CLIP	HEK293	PUM2 SRR048967
PUM2	Hafner *et al.* (2010)	SRR048968	PAR-CLIP	HEK293	PUM2 SRR048968
QKI	Hafner *et al.* (2010)	SRR048969	PAR-CLIP	HEK293	QKI SRR048969
QKI	Hafner *et al.* (2010)	SRR048970	PAR-CLIP	HEK293	QKI SRR048970
ROQUIN	Murakawa *et al.* (2015)	SRR857933	PAR-CLIP	HEK293	ROQUIN SRR857933
ROQUIN	Murakawa *et al.* (2015)	SRR857934	PAR-CLIP	HEK293	ROQUIN SRR857934
SRSF1	Xiao *et al.* (2016)	SRR2107150	PAR-CLIP	HeLa	SRSF1 SRR2107150
SRSF3	Xiao *et al.* (2016)	SRR2107156	PAR-CLIP	HeLa	SRSF3 SRR2107156
SRSF7	Xiao *et al.* (2016)	SRR2107152	PAR-CLIP	HeLa	SRSF7 SRR2107152
SRSF9	Xiao *et al.* (2016)	SRR2107153	PAR-CLIP	HeLa	SRSF9 SRR2107153
ZFP36	Mukherjee *et al.* (2014)	SRR1046759	PAR-CLIP	HEK293	ZFP36 SRR1046759

Protein ID	**SSMART** top 3 sequence-structure motifs
FMR1 SRR527727	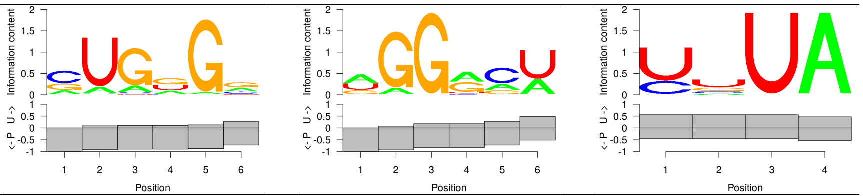
FMR1 SRR527728	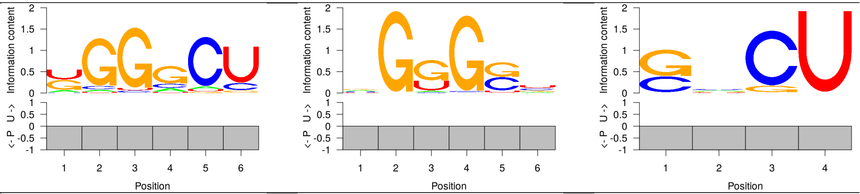
FUS SRR070449	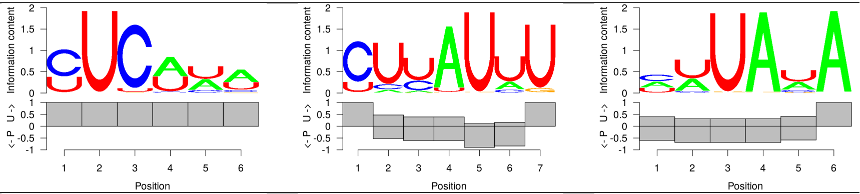
FUS SRR070450	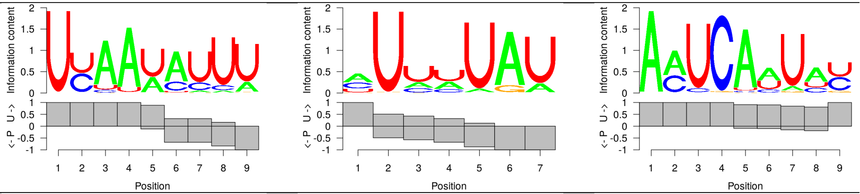
ELAVL1 SRR189777	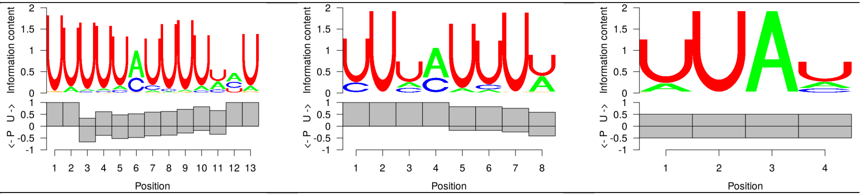
ELAVL1 SRR248532	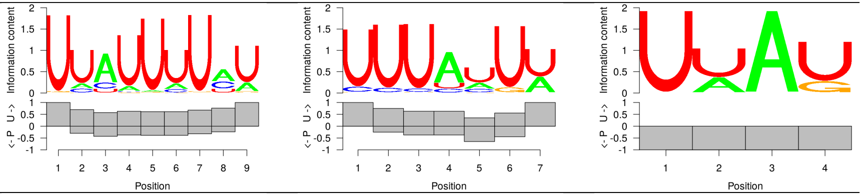
ELAVL1 SRR309285	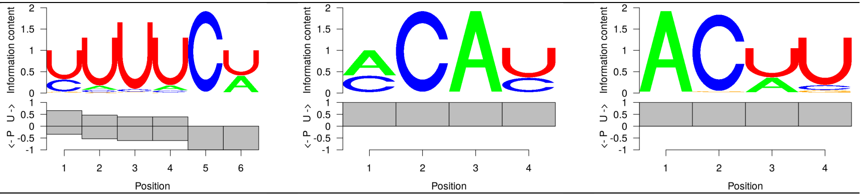
ELAVL1 SRR309286	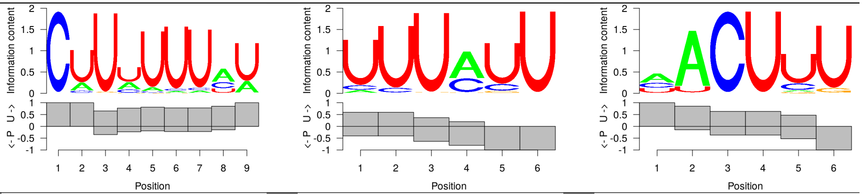
IGF2BP2 SRR048957	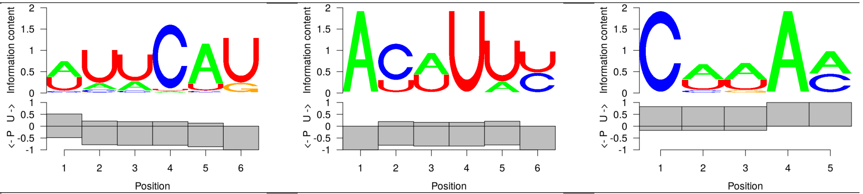
IGF2BP2 SRR048958	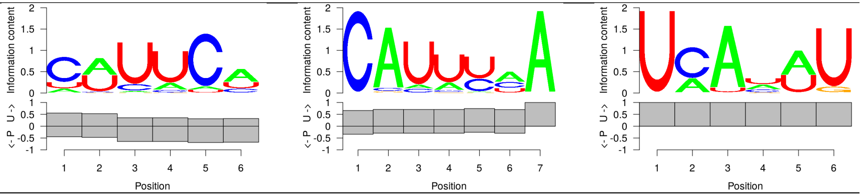

Protein ID	**SSMART** top 3 sequence-structure motifs		
IGF2BP2 SRR048959	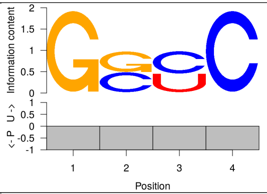	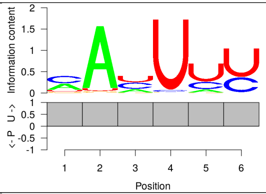	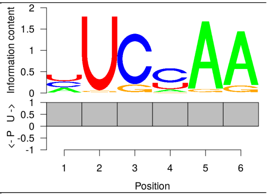
IGF2BP3 SRR048962	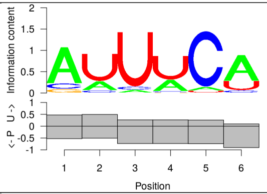	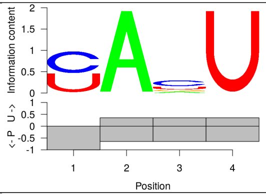	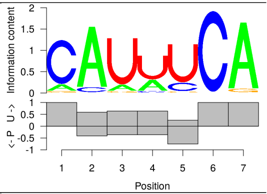
IGF2BP3 SRR048963	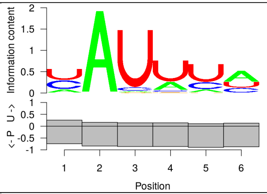	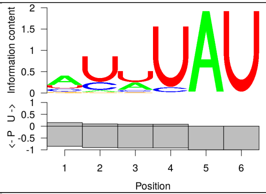	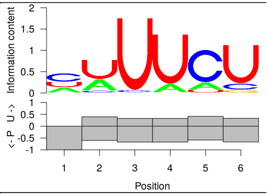
IGF2BP3 SRR048964	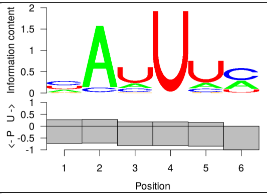	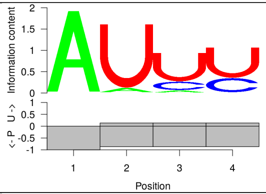	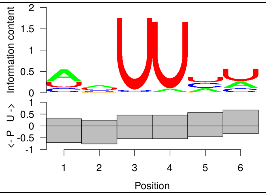
LIN28A-mm SRR458758	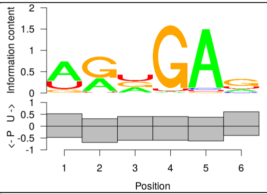	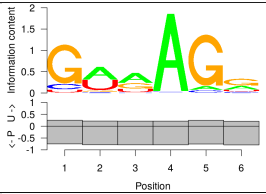	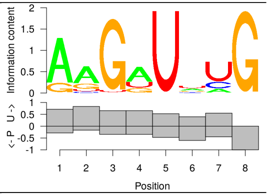
LIN28A-mm SRR458759	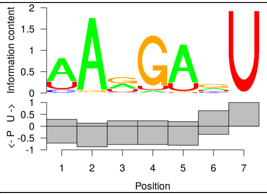	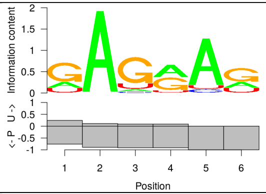	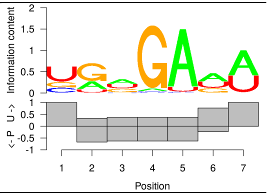
LIN28A-mm SRR458760	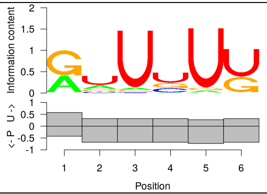	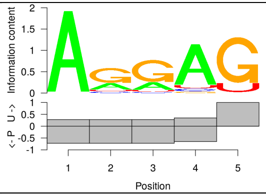	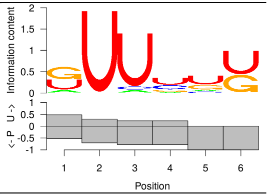
LIN28A SRR531465	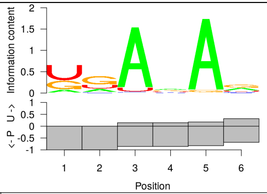	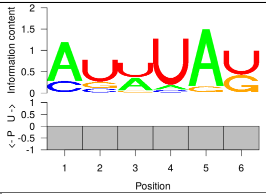	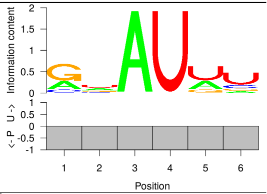
LIN28A SRR531465	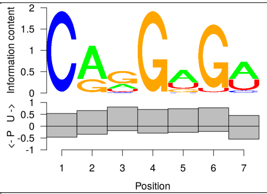	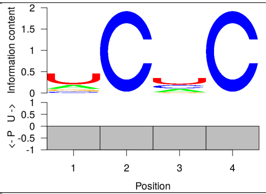	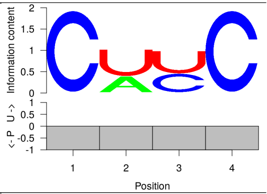
LIN28A SRR764666	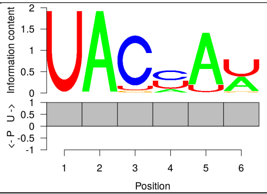	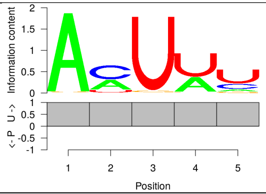	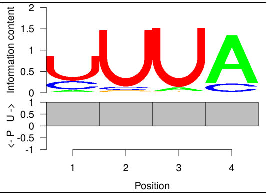

Protein ID	**SSMART** top 3 sequence-structure motifs
LIN28B SRR850551	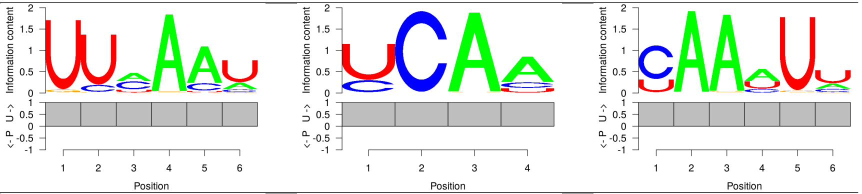
LIN28B SRR850552	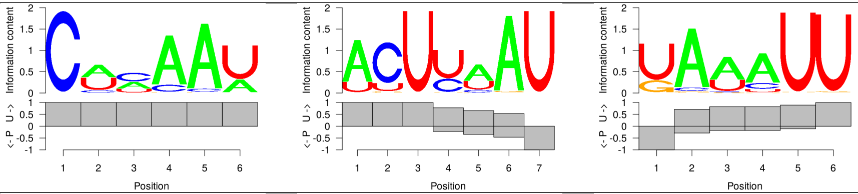
LIN28B SRR764667	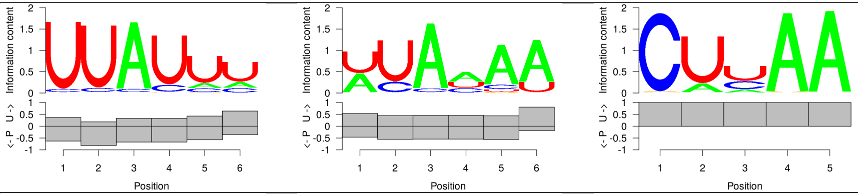
LIN28B SRR764668	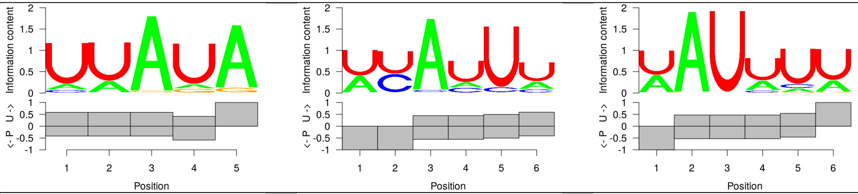
LIN28B SRR764669	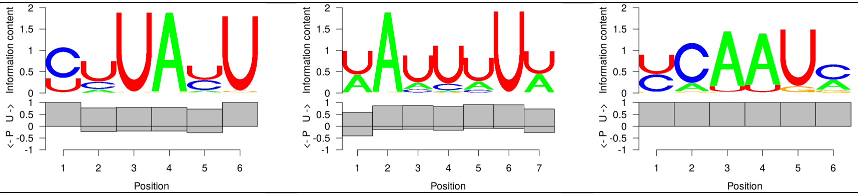
PUM2 SRR048967	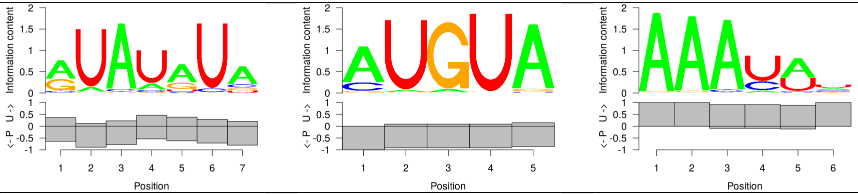
PUM2 SRR048968	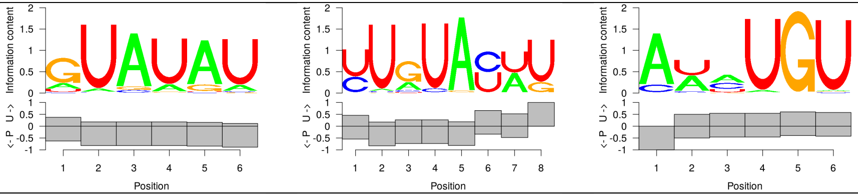
QKI SRR048969	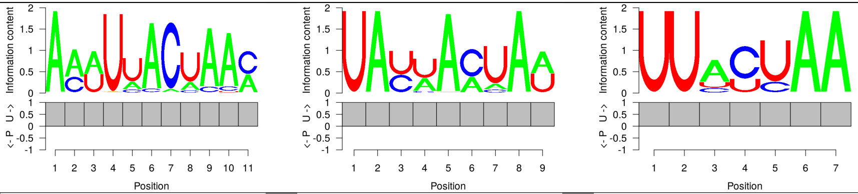
QKI SRR048970	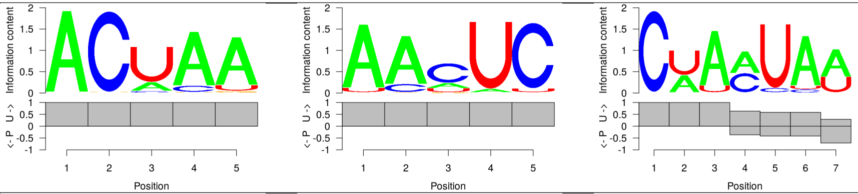
ROQUIN SRR857933	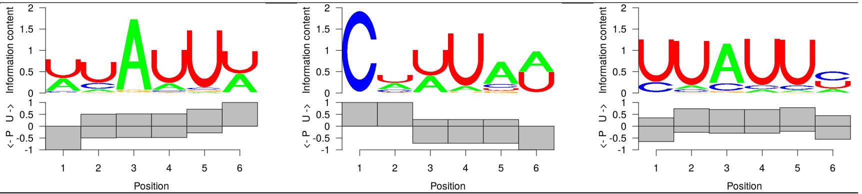

Protein ID	**SSMART** top 3 sequence-structure motifs		
ROQUIN SRR857934	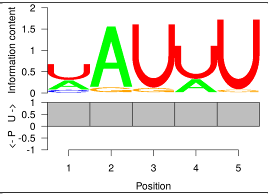	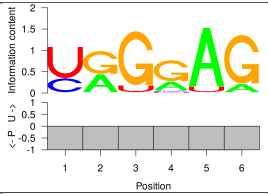	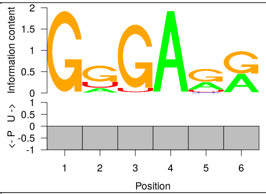
SRSF1 SRR2107150	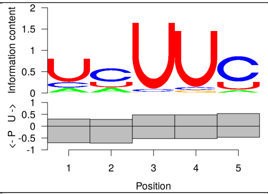	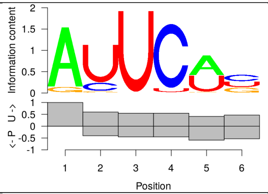	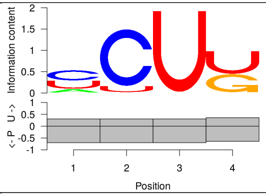
SRSF3 SRR2107156	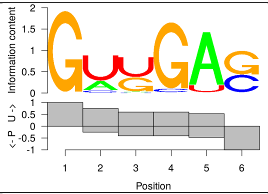	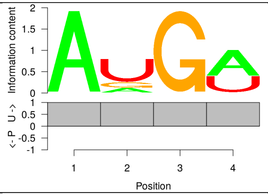	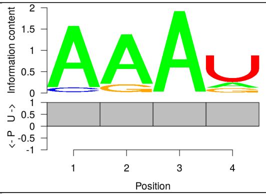
SRSF7 SRR2107152	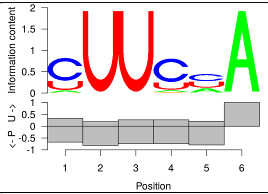	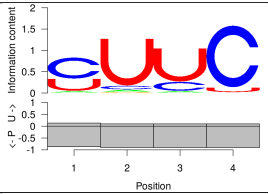	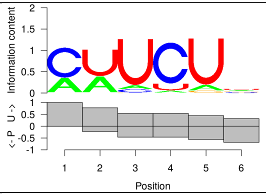
SRSF9 SRR2107153	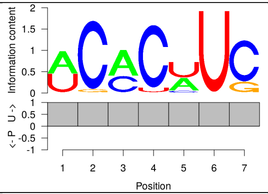	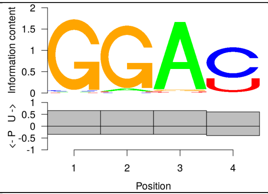	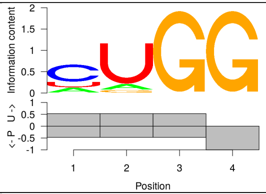
ZFP36 SRR1046759	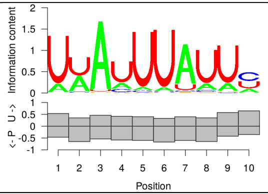	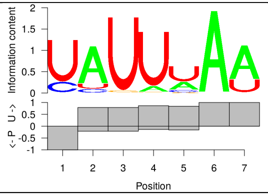	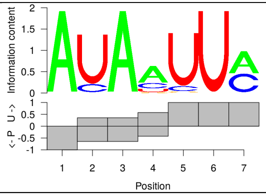

References

Ascano, M., Mukherjee, N., *et al.* (2012). FMRP targets distinct mRNA sequence elements to regulate protein expression. *Nature*, **492**(7429), 382–6.

Bernhart, S. H., Hofacker, I. L., and Stadler, P. F. (2006). Local RNA base pairing probabilities in large sequences. *Bioinformatics*, **22**(5), 614–5.

Cho, J., Chang, H., *et al.* (2012). LIN28A is a suppressor of ER-associated translation in embryonic stem cells. *Cell*, **151**(4), 765–77.

Doshi, K. J., Cannone, J. J., *et al.* (2004). Evaluation of the suitability of free-energy minimization using nearest-neighbor energy parameters for RNA secondary structure prediction. *BMC bioinformatics*, **5**, 105.

Graf, R., Munschauer, M., *et al.* (2013). Identification of LIN28B-bound mRNAs reveals features of target recognition and regulation. *RNA biology*, **10**(7), 1146–59.

Hafner, M., Landthaler, M., *et al.* (2010). Transcriptome-wide identification of RNA-binding protein and microRNA target sites by PAR-CLIP. *Cell*, **141**(1), 129–41.

Hafner, M., Max, K. E. A., *et al.* (2013). Identification of mRNAs bound and regulated by human LIN28 proteins and molecular requirements for RNA recognition. *RNA*, **19**(5), 613–26.

Hoell, J. I., Larsson, E., *et al.* (2011). RNA targets of wild-type and mutant FET family proteins. *Nature structural & molecular biology*, **18**(12), 1428–31.

Kazan, H., Ray, D., *et al.* (2010). RNAcontext: a new method for learning the sequence and structure binding preferences of RNA-binding proteins. *PLoS computational biology*, **6**, e1000832.

Kiryu, H., Terai, G., *et al.* (2011). A detailed investigation of accessibilities around target sites of siRNAs and miRNAs. *Bioinformatics*, **27**(13), 1788–1797.

Kishore, S., Jaskiewicz, L., *et al.* (2011). A quantitative analysis of CLIP methods for identifying binding sites of RNA-binding proteins. *Nature Methods*, **8**(7), 559–564.

Lange, S. J., Maticzka, D., *et al.* (2012). Global or local? Predicting secondary structure and accessibility in mRNAs. *Nucleic acids research*, **40**(12), 5215–26.

Lebedeva, S., Jens, M., *et al.* (2011). Transcriptome-wide analysis of regulatory interactions of the RNA-binding protein HuR. *Molecular cell*, **43**(3), 340–52.

Lekprasert, P., Mayhew, M., and Ohler, U. (2011). Assessing the utility of thermodynamic features for microRNA target prediction under relaxed seed and no conservation requirements. *PloS one*, **6**(6), e20622.

Li, X., Quon, G., *et al.* (2010). Predicting in vivo binding sites of RNA-binding proteins using mRNA secondary structure. *RNA*, **16**(6), 1096–107.

Marin, R. M. and Vanicek, J. (2011). Efficient use of accessibility in microRNA target prediction. *Nucleic Acids Research*, **39**(1), 19–29.

Mukherjee, N., Corcoran, D. L., *et al.* (2011). Integrative regulatory mapping indicates that the RNA-binding protein HuR couples pre-mRNA processing and mRNA stability. *Molecular cell*, **43**(3), 327–39.

Mukherjee, N., Jacobs, N. C., *et al.* (2014). Global target mRNA specification and regulation by the RNA-binding protein ZFP36. *Genome Biology*, **15**(1), R12.

Murakawa, Y., Hinz, M., *et al.* (2015). RC3H1 post-transcriptionally regulates A20 mRNA and modulates the activity of the IKK/NF-κB pathway. *Nature Communications*, **6**, 7367.

Ricci, E. P., Kucukural, A., *et al.* (2014). Staufen1 senses overall transcript secondary structure to regulate translation. *Nature structural & molecular biology*, **21**(1), 26–35.

Rogers, E. and Heitsch, C. E. (2014). Profiling small RNA reveals multimodal substructural signals in a Boltzmann ensemble. *Nucleic acids research*, **42 (22)**, e171.

Wilbert, M. L., Huelga, S. C., *et al.* (2012). LIN28 binds messenger RNAs at GGAGA motifs and regulates splicing factor abundance. *Molecular Cell*, **48**(2), 195–206.

Xiao, W., Adhikari, S., *et al.* (2016). Nuclear m6A Reader YTHDC1 Regulates mRNA Splicing. *Molecular Cell*, **61**(4), 507–519.